

PACS: 87.14.C++c, 87.16.Dg

MOLECULAR DYNAMICS STUDY OF INSULIN MUTANTS

 Olga Zhytniakivska*,  Uliana Tarabara,  Valeriya Trusova,
 Kateryna Vus,  Galyna Gorbenko

Department of Medical Physics and Biomedical Nanotechnologies, V.N. Karazin Kharkiv National University
 4 Svobody Sq., Kharkiv, 61022, Ukraine

*Corresponding Author: olya_zhytniakivska@yahoo.com

Received April 1, 2021; revised April 22, 2021; accepted April 23, 2021

Human insulin, a small protein hormone consisting of A-chain (21 residues) and B-chain (30 residues) linked by three disulfide bonds, is crucial for controlling the hyperglycemia in type I diabetes. In the present work molecular dynamics simulation (MD) with human insulin and its mutants was used to assess the influence of 10 point mutations (His^{A8}, Val^{A10}, Asp^{B10}, Gln^{B17}, Ala^{B17}, Gln^{B18}, Asp^{B25}, Thr^{B26}, Glu^{B27}, Asp^{B28}), 6 double mutations (Glu^{A13}+Glu^{B10}, Ser^{A13}+Glu^{B27}, Glu^{B1}+Glu^{B27}, Ser^{B2}+Asp^{B10}, Asp^{B9}+Glu^{B27}, Glu^{B16}+Glu^{B27}) and one triple mutation (Glu^{A15}+Asp^{A18}+Asp^{B3}) in the protein sequence on the structure and dynamics of human insulin. A series of thermal unfolding MD simulations with wild type (WT) human insulin and its mutants was performed at 400 K with GROMACS software (version 5.1) using the CHARMM36m force field. The MD results have been analyzed in terms of the parameters characterizing both the global and local protein structure, such as the backbone root mean-square deviation, gyration radius, solvent accessible surface area, the root mean-square fluctuations and the secondary structure content. The MD simulation data showed that depending on time evolution of integral characteristics, the examined mutants can be tentatively divided into three groups: 1) the mutants His^{A8}, Val^{A10}, Ala^{B17}, Asp^{B25}, Thr^{B26}, Glu^{B27}, Glu^{A13}+Glu^{B10}, Glu^{B1}+Glu^{B27} and Glu^{B16}+Glu^{B27}, which exert stabilizing effect on the protein structure in comparison with wild type insulin; 2) the mutants Gln^{B17}, Asp^{B10}, Ser^{B2}+Asp^{B10} and Glu^{A15}+Asp^{A18}+Asp^{B3} that did not significantly affect the dynamical properties of human insulin with a minimal stabilizing impact; 3) the mutants Asp^{B28}, Asp^{B9}+Glu^{B27} and Ser^{A13}+Glu^{B27}, Gln^{B18}, destabilizing the protein structure. Analysis of the secondary structure content provided evidence for the influence of Asp^{B28}, Asp^{B9}+Glu^{B27} and Ser^{A13}+Glu^{B27}, Gln^{B18} on the insulin unfolding. Our MD results indicate that the replacement of superficial nonpolar residues in the insulin structure by hydrophilic ones gives rise to the increase in protein stability in comparison with the wild type protein.

KEYWORDS: human insulin, mutants, molecular dynamics simulation, amyloid.

Human insulin, a small protein hormone consisting of an acidic A-chain (21 residues) and a basic B-chain (30 residues) linked by three disulfide bonds, is crucial for controlling the hyperglycemia in type I diabetes [1-3]. However, medical and pharmaceutical applications of this hormone are complicated by its predisposition for aggregation and formation of amyloid fibrils [4-8]. Specifically, it was shown that insulin is capable of forming the amyloid fibrils at the sites of the repeated insulin injection during the therapy of patients with diabetes, thereby inducing the localized insulin-derived amyloidosis (insulin amyloidoma) [4,5]. Moreover, the tendency of insulin to form amyloid fibrils under stressful conditions (elevated temperature, agitation, pH, etc.) represents a serious obstacle during industrial purification, storage and drug delivery of protein-based pharmaceuticals [6,7]. Despite extensive research efforts, the exact molecular details of the insulin amyloid transformation are still under debate. The insulin fibril formation *in vitro* is usually described by the classical nucleation-dependent polymerization model [1,8,9]. However, many other mechanisms for insulin fibrillization have been proposed including the heterogeneous nucleation [10], colloidal coagulation model [9,11] and downhill polymerization [9,11,12].

The *in vitro* oligomerization and aggregation of insulin is essentially controlled by environmental conditions such as pH [13,14], ionic strength [15,16], temperature [14,17,18], the presence of ions [19,20], and protein concentration [14,21]. Previous studies suggested that the early stages of insulin fibrillation are governed mainly by hydrophobic interactions [22,23]. However, several lines of evidence pointed out the importance of the electrostatic interactions in the insulin fibrillization at the initial stage of nucleation [9,23,24]. It is believed that the flexible B-chain of insulin is more important for the protein transition into amyloid state than the rest of molecule [14,23, 25-27]. However, using screening of the amyloid-forming insulin sequence Eisenberg's team suggested at least two protein segments responsible for the insulin amyloid conversion: the L^{B11}VEALYL^{B17} segment of the B-chain accounting for the formation of fibril spine and the S^{A12}LYQLENY^{A19} segment from the A-chain stabilizing the fibril structure [27]. Furthermore, it was showed that the disordered N-terminal segments of both A- and B-chains along with the residues Leu^{B15}, Phe^{B24} and Tyr^{A19} may also contribute to fibril formation [28]. In addition, the surfaces consisting of His^{B10}, Leu^{B17}, Tyr^{B16}, Phe^{B25} and Thr^{A8} were assumed as the potential sites that trigger insulin fibrillization [14,28]. Notably, both A- and B-chains of insulin by their own are capable of forming the amyloid fibrils under denaturing conditions [24]. Intriguingly, the mutations in the C-terminus of human insulin B-chain were reported to affect the amyloidogenic propensity of the protein [14,29-31]. Specifically, the removal of five residues from the B-chain led to the enhancement of insulin fibrillization [14], while the mutants T30R and K29R/T30R showed different resistance against stress-induced fibril growth on the initial stage of nucleation [23]. Furthermore, the delay in the lag phase of insulin fibrillization was observed for the point mutations H10D and L17Q [31], whereas the substitution of Pro^{B28} with (4S)-hydroxyproline (Hzp) resulted in the higher resistance to fibril formation [32].

The aim of the present study was to assess the influence 10 point mutations (His^{A8} , Val^{A10} , Asp^{B10} , Gln^{B17} , Ala^{B17} , Gln^{B18} , Asp^{B25} , Thr^{B26} , Glu^{B27} , Asp^{B28}), 6 double mutations ($\text{Glu}^{\text{A13}}+\text{Glu}^{\text{B10}}$, $\text{Ser}^{\text{A13}}+\text{Glu}^{\text{B27}}$, $\text{Glu}^{\text{B1}}+\text{Glu}^{\text{B27}}$, $\text{Ser}^{\text{B2}}+\text{Asp}^{\text{B10}}$, $\text{Asp}^{\text{B9}}+\text{Glu}^{\text{B27}}$, $\text{Glu}^{\text{B16}}+\text{Glu}^{\text{B27}}$) and one triple mutation ($\text{Glu}^{\text{A15}}+\text{Asp}^{\text{A18}}+\text{Asp}^{\text{B3}}$) in the human insulin sequence on the protein structure and dynamics. To this end, a series of thermal unfolding MD simulations with wild type (WT) protein and its mutants was performed.

MOLECULAR DYNAMICS SIMULATIONS

The molecular dynamics simulations were conducted with GROMACS software (version 5.1) using the CHARMM36m force field with TIP3P water model [33]. The starting structure for simulations was taken from the Protein Data Bank (PDB entry for human insulin 3I3Z). The mutations His^{A8} , Val^{A10} , Asp^{B10} , Gln^{B17} , Ala^{B17} , Gln^{B18} , Asp^{B25} , Thr^{B26} , Glu^{B27} , Asp^{B28} , $\text{Glu}^{\text{A13}}+\text{Glu}^{\text{B10}}$, $\text{Ser}^{\text{A13}}+\text{Glu}^{\text{B27}}$, $\text{Glu}^{\text{B1}}+\text{Glu}^{\text{B27}}$, $\text{Ser}^{\text{B2}}+\text{Asp}^{\text{B10}}$, $\text{Asp}^{\text{B9}}+\text{Glu}^{\text{B27}}$, $\text{Glu}^{\text{B16}}+\text{Glu}^{\text{B27}}$, $\text{Glu}^{\text{A15}}+\text{Asp}^{\text{A18}}+\text{Asp}^{\text{B3}}$ were introduced to the protein sequence using the web-based graphical interface CHARMM-GUI. The input files for MD calculations were prepared using the CHARMM-GUI Quick MD simulator [34].

The human insulin and its mutants were solvated in the rectangular box fitted to protein size. The minimal distance from the protein molecule to the box edges was 10 Å. To obtain a neutral total charge of the system the required amount of positive ions was added. The number of atoms in the solvated protein systems varied from 14670 to 17573. The Particle Mesh Ewald algorithm was used to treat the long-range electrostatic interactions [35]. The minimization and equilibration of the system were performed during 100 ps and 500 ps, respectively. The time step for MD simulations was 2 fs. The trajectories and coordinates were saved every 2 ps for further analysis. The whole time interval for MD calculations was 100 ns. The MD simulations of the human insulin and its mutants were performed at 400 K and a pressure 1 bar. The analysis tools provided by GROMACS were used to calculate the root mean-square deviations (RMSD), root mean-square fluctuations of the C-alpha atoms (RMSF), radius of gyration (Rg) and solvent-accessible surface area (SASA) per residue. The evolution of the secondary structure was followed using the VMD Timeline tool [36] and Tcl scripts.

RESULTS AND DISCUSSION

To examine the changes in the conformational behaviour of the mutated human insulin as compared to its wild type counterpart we analysed the thermal unfolding trajectories by calculating the parameters reflecting the changes in both the global and local protein structure (RMSD, Rg, SASA, RMSF) and the secondary structure content. Fig. 1 shows the changes of the backbone root mean square deviations with time.

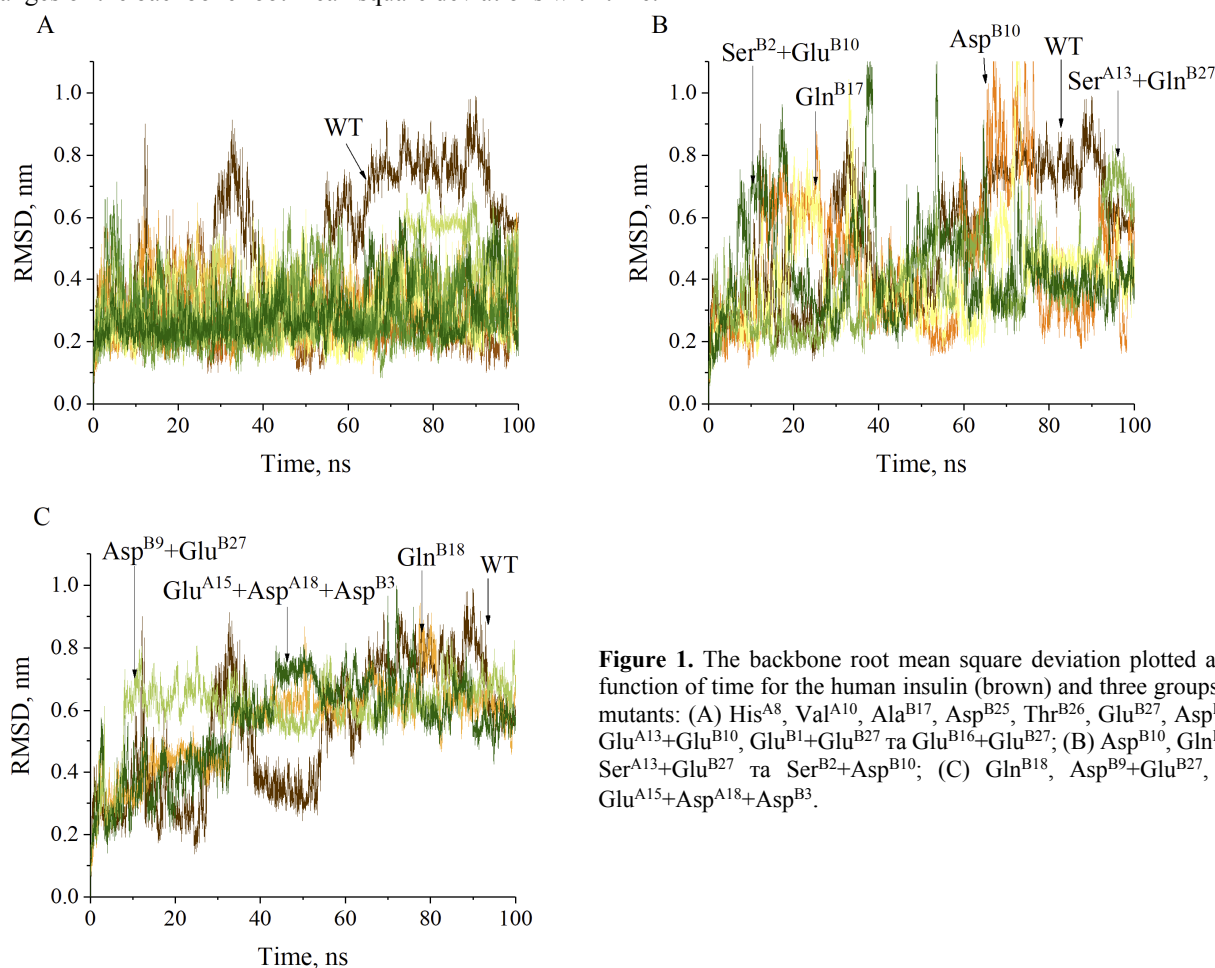


Figure 1. The backbone root mean square deviation plotted as a function of time for the human insulin (brown) and three groups of mutants: (A) His^{A8} , Val^{A10} , Ala^{B17} , Asp^{B25} , Thr^{B26} , Glu^{B27} , Asp^{B28} , $\text{Glu}^{\text{A13}}+\text{Glu}^{\text{B10}}$, $\text{Glu}^{\text{B1}}+\text{Glu}^{\text{B27}}$ and $\text{Glu}^{\text{B16}}+\text{Glu}^{\text{B27}}$; (B) Asp^{B10} , Gln^{B17} , $\text{Ser}^{\text{A13}}+\text{Glu}^{\text{B27}}$ and $\text{Ser}^{\text{B2}}+\text{Asp}^{\text{B10}}$; (C) Gln^{B18} , $\text{Asp}^{\text{B9}}+\text{Glu}^{\text{B27}}$, and $\text{Glu}^{\text{A15}}+\text{Asp}^{\text{A18}}+\text{Asp}^{\text{B3}}$.

As seen in Fig. 2, the calculated RMSD values for human insulin and its mutants do not exceed 1 nm, except short-time fluctuations of Asp^{B10}, Gln^{B17} and Ser^{B2}+Asp^{B10}. Notably, for the WT insulin the time dependence of RMSD is characterized by four periods: 1) strong fluctuations ~ 0.3 nm with deviations up to 0.9 nm during the first 25 ns of simulation; 2) a slight increase of RMSD values to 0.66-0.78 nm during the next 3ns followed by the fluctuations at this level during ~ 8 ns; 3) substantial decrease of RMSD values to 0.33-0.38 nm starting from ~36 ns; 4) gradual RMSD increase to 0.6-0.8 nm remaining almost stable during the last 50 ns of the simulation. The RMSDs of mutants His^{A8}, Val^{A10}, Ala^{B17}, Asp^{B25}, Thr^{B26}, Glu^{B27}, Asp^{B28}, Glu^{A13}+Glu^{B10}, Glu^{B1}+Glu^{B27} and Glu^{B16}+Glu^{B27} were significantly lower during the simulation time compared with the WT insulin. As seen in Fig. 2, the mutants Gln^{B18}, Asp^{B9}+Glu^{B27} and Glu^{A15}+Asp^{A18}+Asp^{B3} showed higher RMSDs during the first 60 ns of the simulation relative to WT protein and similar type of deviations throughout the following 40 ns of RMSD trajectories. In turn, the simulation of mutants Asp^{B10}, Gln^{B17}, Ser^{A13}+Glu^{B27} and Ser^{B2}+Asp^{B10} produced less stable trajectories in comparison with WT insulin.

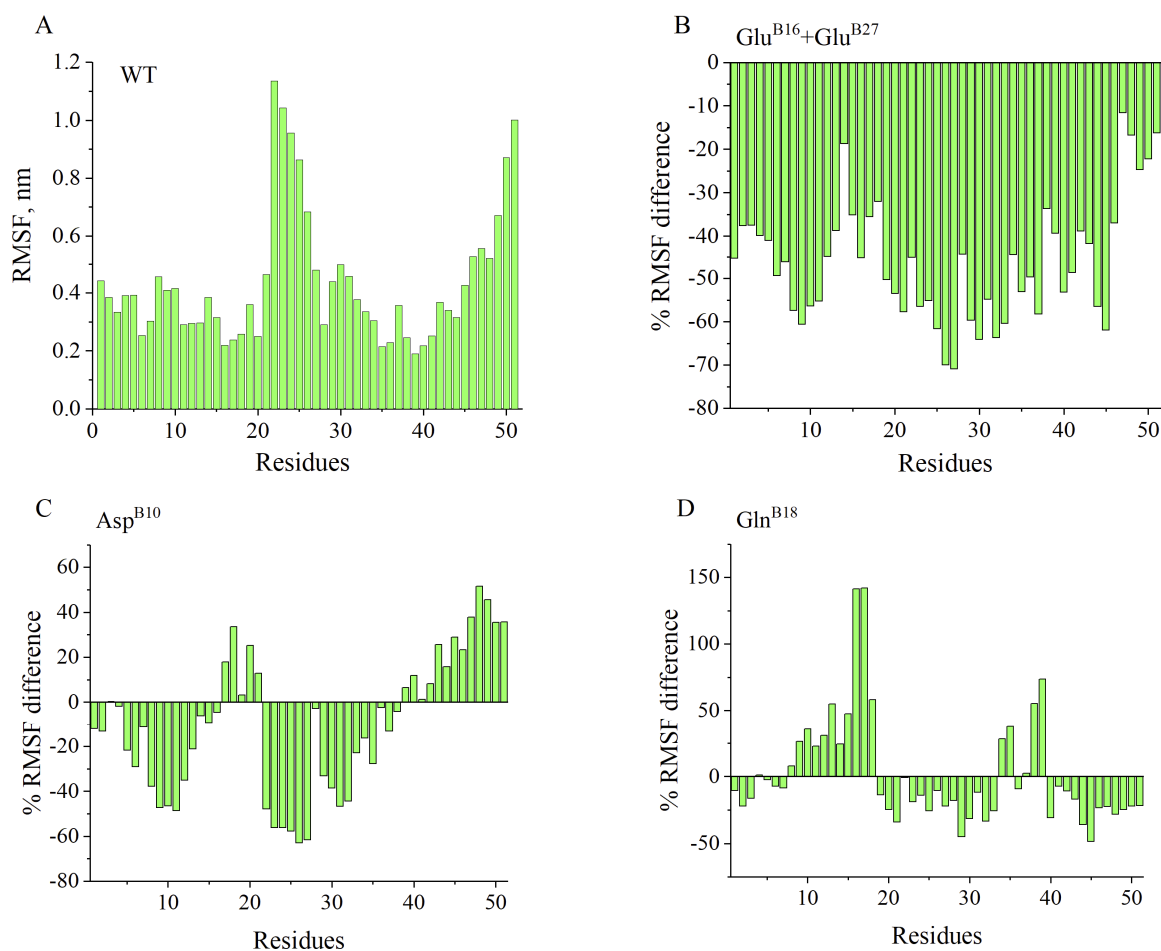


Figure 2. The root mean square fluctuations of the C-alpha atoms of WT insulin(A) and the relative changes in root-mean-square fluctuations for Glu^{B16}+Glu^{B27} (B), Asp^{B10} (C), Gln^{B18} (D) insulin mutants, calculated as $\left(\frac{RMSF_{mut}}{RMSF_{WT}} - 1\right) \cdot 100\%$.

To determine how the mutations affect the dynamic behavior of amino acid residues, the RMSF values of the C-alpha atoms of WT insulin and mutants were calculated (Fig. 2). The RMSF values for the majority of the WT protein residues ranged from 0.2 to 0.5 nm during the simulation (Fig. 2.A). The only exception were the residues 22-26 (RMSFs vary from 0.68 to 1.14 nm) representing the first five residues of the N-terminal region of B-chain, and the residues 46-51 (RMSFs vary from 0.52 to 1.0 nm), belonging to the end of the C-terminal of this chain. The analysis of the relative changes in RMSF revealed that both N- and C-terminal regions of B-chain in all mutants fluctuate stronger than in the WT insulin with the magnitude of this effect being dependent on the type of mutation (data not shown). More specifically, there are three main tendencies in the relative changes of RMSF, according to which all examined mutants can be divided into three groups. The representatives of the first group (Val^{A10}, Ala^{B17}, Asp^{B28}, Ser^{A13}+Glu^{B27}, Glu^{B1}+Glu^{B27} and Asp^{B9}+Glu^{B27}) are characterized by strong fluctuations of similar amplitudes on both N- and C-terminal regions of B-chain. The second group contains Gln^{B18}, Glu^{B27} and Glu^{A15}+Asp^{A18}+Asp^{B3} mutants which, like WT insulin, display significantly higher fluctuations in the N-terminal region in comparison with C-terminal part of B-chain. For all other mutants under study (the third group) the relative changes of RMSF values were opposite to those observed for the second

group. The obtained results are in good agreement with the experimental evidence for the higher conformational flexibility of B-chain with respect to the rest of the protein [29,31].

Notably, some mutants have significantly larger fluctuations in A-chain residues compared to the 7-22 sequence of the core of B-chain. Specifically, higher RMSFs were observed for Val^{A10} (1-5, 13-15 and 18-19 A-chain residues), Gln^{B18} (8-10 and 13-18 A-chain residues), Asp^{B25} (1-5, 10 and 12-15 A-chain residues), Asp^{B28} (1-5 and 12-15 A-chain residues), Ser^{A13}+Glu^{B27} (1-5 and 11-14 A-chain residues), Ser^{B2}+Asp^{B10} (1-4 and 14 A-chain residues), Glu^{A15}+Asp^{A18}+Asp^{B3} (8-10 A-chain residues). Remarkably, although the above results demonstrate the increase in RMSFs (in comparison with B-chain) for the polypeptide fragment consisting of 8-19 residues responsible for the stabilization of insulin fibrils [28,30], the mutations didn't significantly modify the conformation of this region, since the mutated and WT insulin showed nearly similar RMSFs for this sequence of residues.

It has been suggested previously that local unfolding of the B11-B17 fragment of insulin causes the increase in fibrillation rate [37]. However, as seen in Fig. 2 (panels B-D) the fluctuations of these residues were even smaller than those for WT protein. Nevertheless, the comparison of the relative changes in root-mean-square fluctuations of WT insulin and its mutants indicates the stabilizing effect of mutations His^{A8}, Val^{A10}, Ala^{B17}, Asp^{B25}, Thr^{B26}, Glu^{B27}, Glu^{A13}+Glu^{B10}, Glu^{B1}+Glu^{B27} and Glu^{B16}+Glu^{B27} on virtually all protein residues (the relative changes in root-mean-square fluctuations \leq 74%). Notably, the highest fluctuations were observed for the variant Gln^{B18} which is characterized by the increase of A16 and A17 RMSFs to \sim 141% compared to WT insulin. The analysis of the relative changes in the RMSF revealed that the region B20-B30 fluctuates stronger in the mutants Glu^{A15}+Asp^{A18}+Asp^{B3} (\sim 39%), Gln^{B17} (\sim 67%), Asp^{B10} (\sim 52%), Ser^{A13}+Glu^{B27} (\sim 65%), Ser^{B2}+Asp^{B10} (\sim 66%) and Gln^{B18} (\sim 73%) than in the WT protein. The mutants Asp^{B28}, Ser^{A13}+Glu^{B27}, Gln^{B18} have significantly larger fluctuations in the A8-A18 region, with RMSF difference ranging from \sim 35% to \sim 72%. By considering the amount of residues fluctuating stronger than in the WT protein, along with the maximal positive and negative relative RMSF changes, we observed that the destabilizing impact of mutants on the protein dynamics increases in the following row: Asp^{B25} < Asp^{B9}+Glu^{B27} < Glu^{A15}+Asp^{A18}+Asp^{B3} < Gln^{B17} < Asp^{B28} < Asp^{B10} < Ser^{A13}+Glu^{B27} < Ser^{B2}+Asp^{B10} < Gln^{B18}.

Fig. 3 represents the time-course evolution of the radius of gyration.

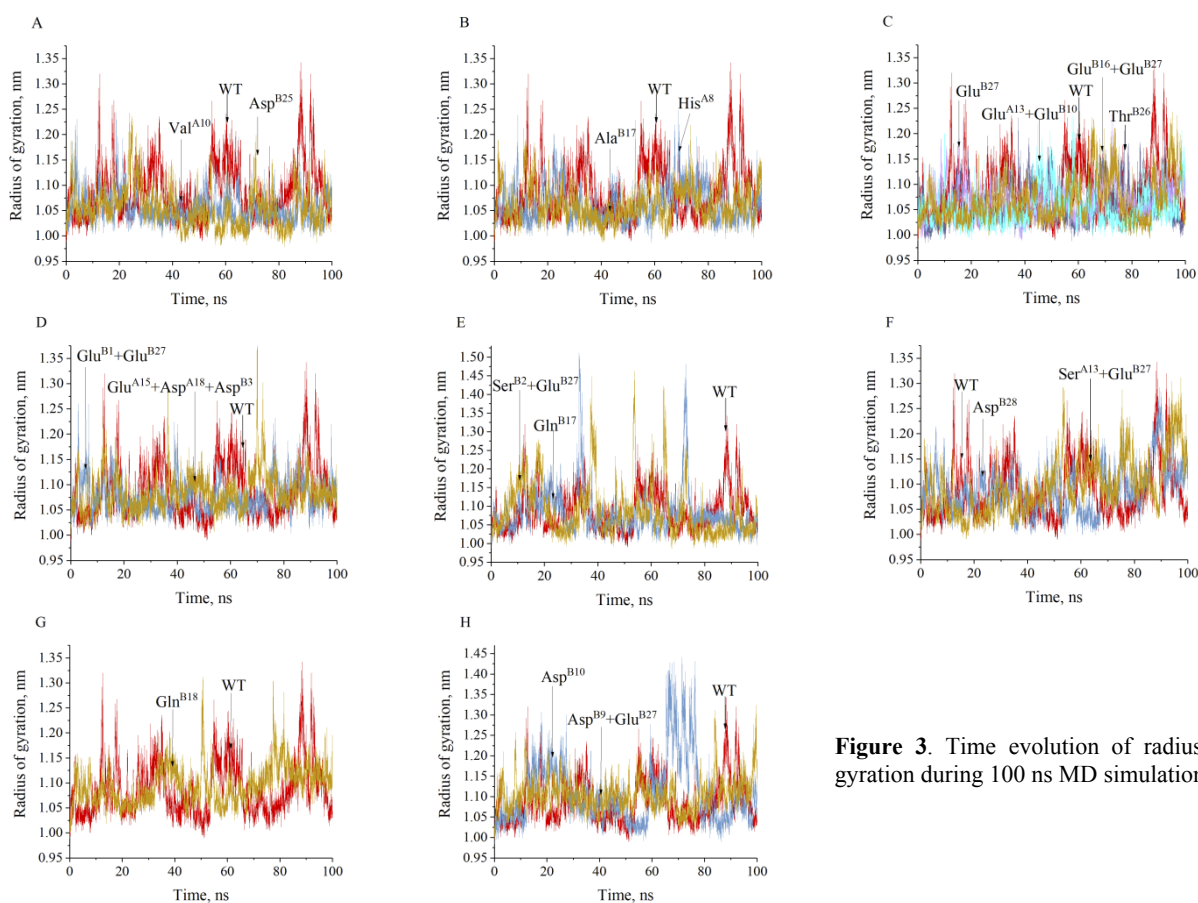


Figure 3. Time evolution of radius of gyration during 100 ns MD simulations.

The Rg value of the WT insulin rises from \sim 1 to \sim 1.34 nm. The approximation of the time dependence of the radius of gyration by the linear function showed that the slope of graph increases with time from \sim 1.07 nm at the beginning of simulation to \sim 1.1 nm at 100 ns. Since the gyration radius correlates with the extent of protein unfolding, the approximation of the time evolution of the radius of gyration by the linear function allowed us to identify the three groups of mutants. The first group contains Glu^{A13}+Glu^{B10}, Glu^{B16}+Glu^{B27}, Thr^{B26}, Glu^{B27}, His^{A8}, Ala^{B17}, Val^{A10}, and Asp^{B25} whose

approximation lines are positioned below the approximation line of WT protein (Fig. 2.A-C). The second group includes $\text{Glu}^{\text{B1}}+\text{Glu}^{\text{B27}}$, $\text{Glu}^{\text{A15}}+\text{Asp}^{\text{A18}}+\text{Asp}^{\text{B3}}$, $\text{Ser}^{\text{B2}}+\text{Asp}^{\text{B10}}$, Gln^{B17} , Asp^{B28} , $\text{Ser}^{\text{A13}}+\text{Glu}^{\text{B27}}$ and Gln^{B18} , whose approximation lines are comparable with that for WT protein (Fig. 2.E-F), while Gln^{B1} , Asp^{B10} and $\text{Asp}^{\text{B9}}+\text{Glu}^{\text{B27}}$ with approximation lines located significantly higher than that for WT insulin constitute the third group.

To assess the alterations in the environment of hydrophobic residues during the simulation, we concentrated on the relative changes in the solvent accessible surface area per residue SASA (Fig. 4). For WT insulin the SASA values do not exceed 1.8 nm. We found that polar A5, A8, A21, B4, positively charged (B5, B10, B22, B29), negatively charged (A4, B13, B21), aromatic (A14, B1, B16, B25, B26) and three nonpolar residues (A10, B17 or B30) are highly accessible to the solvent during the simulation time (Fig. 4). Notably, the profiles of SASA per residue were similar for mutated and WT insulin, indicating that A14, B1, B21 and B29 residues are more accessible to water than the other residues in the protein sequence. Considering the number of residues whose SASA values are higher relative to WT protein, the examined mutants were found to follow the order: $\text{Ala}^{\text{B17}} = \text{Glu}^{\text{B27}} < \text{Glu}^{\text{B16}}+\text{Glu}^{\text{B27}} < \text{Val}^{\text{A10}}$, $\text{Glu}^{\text{A13}}+\text{Glu}^{\text{B10}} = \text{Thr}^{\text{B26}} = \text{His}^{\text{A8}}$, $\text{Gln}^{\text{B18}} < \text{Glu}^{\text{B1}}+\text{Glu}^{\text{B27}} = \text{Asp}^{\text{B25}} < \text{Gln}^{\text{B17}} < \text{Ser}^{\text{A13}}+\text{Glu}^{\text{B27}} < \text{Asp}^{\text{B28}}$, $\text{Ser}^{\text{B2}}+\text{Asp}^{\text{B10}} = \text{Glu}^{\text{A15}}+\text{Asp}^{\text{A18}}+\text{Asp}^{\text{B3}} < \text{Asp}^{\text{B9}}+\text{Glu}^{\text{B27}} = \text{Asp}^{\text{B10}}$.

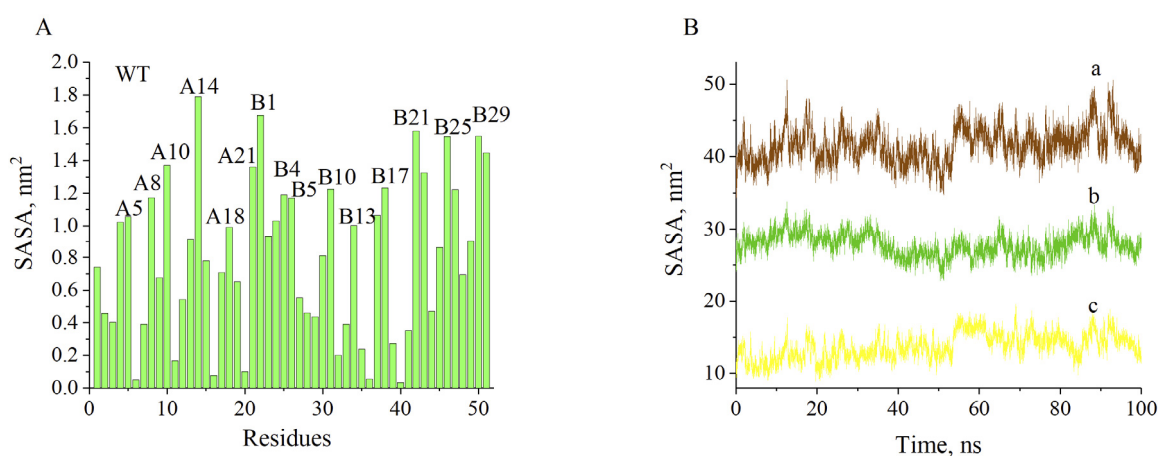


Figure 4. The solvent accessible surface area per residue (A) and time evolution of SASA (B) for whole protein (a), its hydrophobic (b) and hydrophilic (c) residues calculated for wild type insulin.

Notably, depending on the decrease or increase of SASA relative to WT protein, all residues can be divided into two groups. The first group includes the residues A4, A7, A17, A20, B1, B7, B9, B12, B13, B16-B22, B47 and B29, whose SASA is greater than that of WT insulin. In turn, the residues of the second group (A1-A3, A5, A6, A8-A14, A16, A19, A21, B2-B6, B8, B10, B11, B14, B15, B23-B25, B28, B30) are characterized by lower SASA values. Remarkably, the hydrophobic residues represent ~ 32% and ~ 63% of all residues in the first and second groups, respectively, being indicative of the decreased solvent accessibility of nonpolar and aromatic residues of mutants in comparison with WT protein.

To take a closer look on the impact of hydrophobic and hydrophilic residues on the solvent accessible surface area, the time evolution of SASA values was analyzed for: 1) all protein residues; 2) hydrophobic residues; and 3) hydrophilic residues (Fig. 4.B). The approximation of the time-course SASA evolution by the linear function for all protein residues and independently for hydrophobic and hydrophilic residues showed that:

- 1) The growth of the total SASA value with time is caused by the increase of both the hydrophobic and hydrophilic SASAs for Asp^{B10} , Ala^{B17} , Gln^{B18} , Thr^{B26} , Asp^{B28} , $\text{Glu}^{\text{A13}}+\text{Glu}^{\text{B10}}$, $\text{Ser}^{\text{A13}}+\text{Glu}^{\text{B27}}$ or $\text{Glu}^{\text{B16}}+\text{Glu}^{\text{B27}}$;
- 2) The increase of the total SASA value with time for the wild type protein and the mutants Glu^{B27} , $\text{Glu}^{\text{A15}}+\text{Asp}^{\text{A18}}+\text{Asp}^{\text{B3}}$, $\text{Asp}^{\text{B9}}+\text{Glu}^{\text{B27}}$ results from the increase of the solvent accessibility of hydrophobic residues;
- 3) A slight increase of the total SASA for His^{A8} and $\text{Glu}^{\text{B1}}+\text{Glu}^{\text{B27}}$ reflects the increase of the solvent accessibility of hydrophilic residues;
- 4) The decrease of the total SASA with time observed for Gln^{B17} , originates from the reduction of SASAs for hydrophilic residues;
- 5) The solvent accessibility of both hydrophobic and hydrophilic residues reduces for Val^{A10} , Asp^{B25} and $\text{Ser}^{\text{B2}}+\text{Asp}^{\text{B10}}$

The above results indicate that the replacement of superficial nonpolar residues by hydrophilic ones increases the insulin stability in comparison with the wild type protein.

Next, to clarify the effect of mutations on the insulin unfolding pathway, we analyzed the time course of the changes in protein secondary structure through determining the percentage of residues adopting the α -helix, β -sheet or 3_{10} -helix conformations during the simulation (Table 1). It appeared that the content of α -helices rises from 35% to 50% in the following row: $\text{Asp}^{\text{B9}}+\text{Glu}^{\text{B27}} < \text{Gln}^{\text{B18}} < \text{Ser}^{\text{A13}}+\text{Glu}^{\text{B27}} < \text{Asp}^{\text{B28}} < \text{Asp}^{\text{B25}} < \text{Glu}^{\text{B16}}+\text{Glu}^{\text{B27}} < \text{Glu}^{\text{B1}}+\text{Glu}^{\text{B27}} < \text{Val}^{\text{A10}} < \text{Thr}^{\text{B26}} < \text{Ala}^{\text{B17}} < \text{His}^{\text{A8}} < \text{Glu}^{\text{B27}} < \text{Glu}^{\text{A13}}+\text{Glu}^{\text{B10}} < \text{WT} < \text{Glu}^{\text{A15}}+\text{Asp}^{\text{A18}}+\text{Asp}^{\text{B3}} < \text{Ser}^{\text{B2}}+\text{Asp}^{\text{B10}} <$

Asp^{B10} < Gln^{B17}. Given that the native insulin contains 3 α -helices (47%), the above results can be explained either by the destruction of α -helices during the simulation or the appearance of the additional α -helix conformations. In turn, we observed only small percentage of β -sheets (absent in the native conformation) increasing in the order: Asp^{B9}+Glu^{B27} < Glu^{A15} < Asp^{A18}+Asp^{B3} < Val^{A10} < WT < Gln^{B18} < Ser^{B2}+Asp^{B10} < Thr^{B26} < Ala^{B17} < Asp^{B25} < Asp^{B10} < His^{A8} < Glu^{B27} < Glu^{B16}+Glu^{B27} < Ser^{A13}+Glu^{B27} < Asp^{B28} < Glu^{A13}+Glu^{B10} < Gln^{B17} < Glu^{B1}+Glu^{B2}.

Table 1. The percentage of residues adopting α -helix, β -sheet or 3_{10} -helix conformations during the simulation

Protein	β -sheet	α -helix	3_{10} -helix
WT	0.04	46.0	3.1
His ^{A8}	0.18	45.0	1.7
Val ^{A10}	0.02	44.5	2.7
Asp ^{B10}	0.16	47.0	1.7
Gln ^{B17}	1.73	50.0	1.2
Ala ^{B17}	0.08	44.9	2.4
Gln ^{B18}	0.04	36.1	4.6
Asp ^{B25}	0.15	43.7	2.1
Thr ^{B26}	0.08	44.7	3.1
Glu ^{B27}	0.24	45.7	2.5
Asp ^{B28}	0.72	38.6	3.7
Glu ^{A13} +Glu ^{B10}	0.87	45.8	1.5
Ser ^{A13} +Glu ^{B27}	0.30	37.0	3.7
Glu ^{B1} +Glu ^{B27}	2.08	44.5	2.9
Ser ^{B2} +Asp ^{B10}	0.08	47.5	1.3
Asp ^{B9} +Glu ^{B27}	0	34.7	5.0
Glu ^{B16} +Glu ^{B27}	0.30	44.3	2.6
Glu ^{A15} + Asp ^{A18} +Asp ^{B3}	0	46.7	4.3

To characterize the changes in the secondary structure of mutants during the simulation, we analyzed the time evolution of α -helices (Fig. 6). The wild type insulin was characterized by the fluctuations of the α -helices content at the level $\sim 42\%$ (first 25 ns of simulation), followed by the substantial increase of the percentage of α -helices till $\sim 60\%$ during the next 15 ns period, after which a slight helicity decrease was observed until achievement of the initial level of fluctuations to the end of the simulation. The curve of the time evolution of α -helices for Glu^{A15}+ Asp^{A18}+Asp^{B3} was almost identical to that for WT protein. Moreover, the fluctuations of the α -helices content from $\sim 33\%$ till $\sim 51\%$ was observed for Glu^{B1}+Glu^{B27}, Glu^{B16}+Glu^{B27}, His^{A8}, Val^{A10}, Ala^{B17}, Thr^{B26}, Glu^{B27}, Glu^{A13}+Glu^{B10}, reflecting the stability of their secondary structure during the simulation.

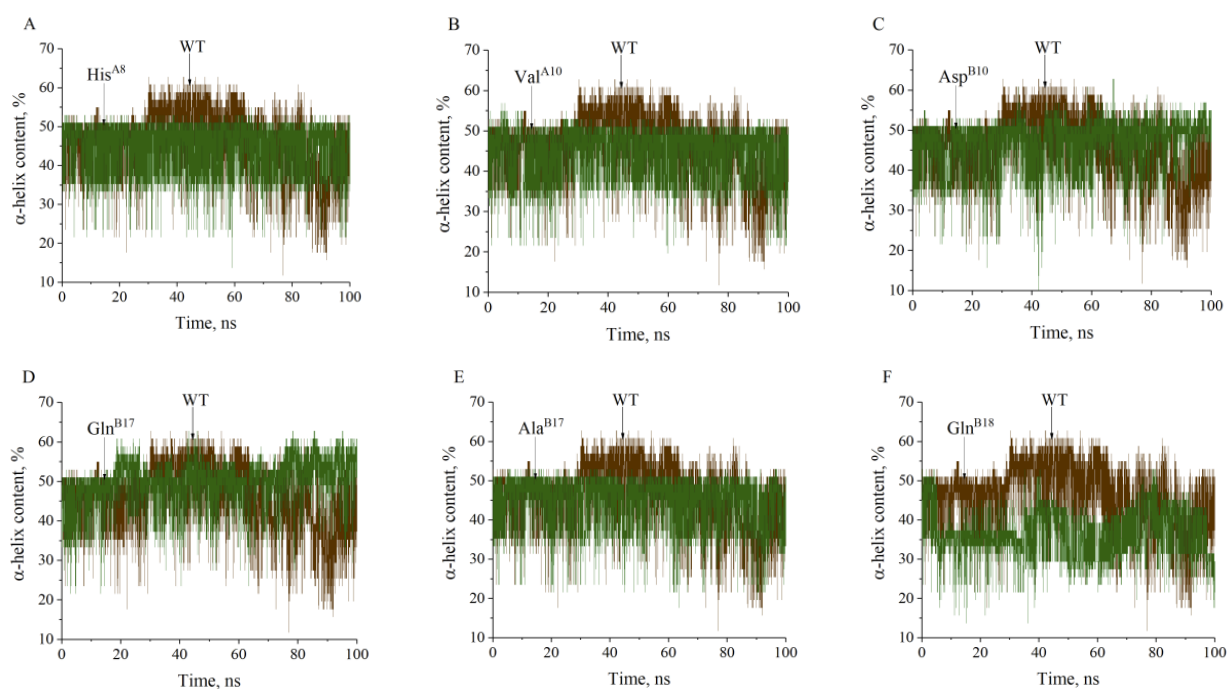


Figure 6. Time evolution of the α -helices of wild type protein (brown) and mutants (green)
(continued on next page)

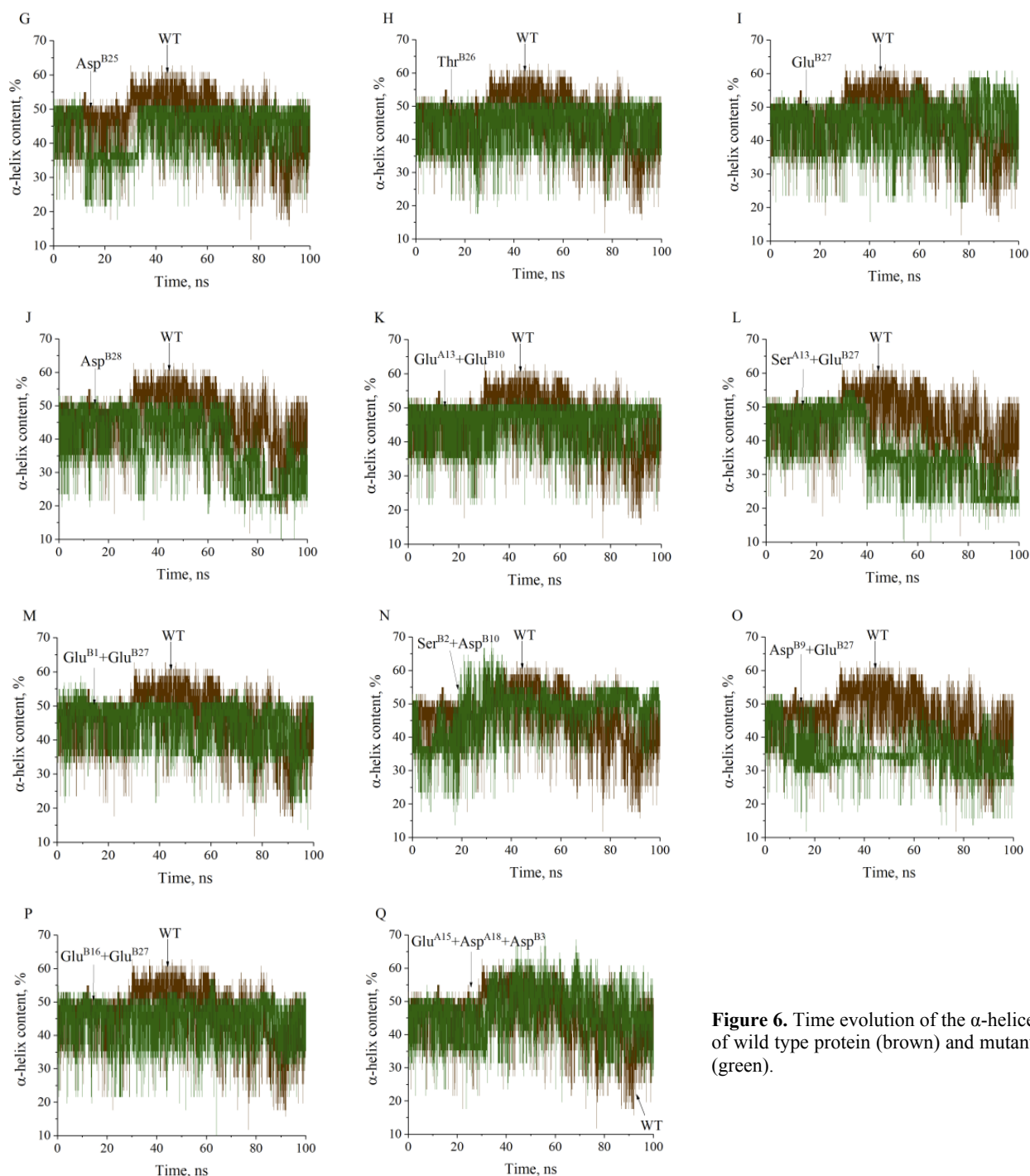


Figure 6. Time evolution of the α -helices of wild type protein (brown) and mutants (green).

In turn, a slight increase of the percentage of α -helices was observed for Asp^{B10} (till ~ 47-54 %) and Gln^{B17} (till ~ 46-61 %) during the simulation. Notably, the decrease of the α -helices content with time was inherent to Asp^{B25} (~ 25-38% during the period 11-33 ns), Asp^{B28} (~ 22-36% from the 70 ns), Ser^{A13}+Glu^{B27} (~ 22-36 starting after 38 ns), Gln^{B18} (~ 29-46 % beginning from 5 ns) and Asp^{B9}+Glu^{B27} (~ 28-44% 36 starting after 7 ns). The analysis of the secondary structure content evidenced a higher unfolding extent of Asp28, AspB9+GluB27, SerA13+GluB27, GlnB18 in comparison with the WT protein.

CONCLUSIONS






To summarize, the present study indicates that introduction of 10 point mutations (His^{A8}, Val^{A10}, Asp^{B10}, Gln^{B17}, Ala^{B17}, Gln^{B18}, Asp^{B25}, Thr^{B26}, Glu^{B27}, Asp^{B28}), 6 double mutations (Glu^{A13}+Glu^{B10}, Ser^{A13}+Glu^{B27}, Glu^{B1}+Glu^{B27}, Ser^{B2}+Asp^{B10}, Asp^{B9}+Glu^{B27}, Glu^{B16}+Glu^{B27}) and one triple mutation (Glu^{A15}+Asp^{A18}+Asp^{B3}) in the protein sequence has different impact on the structural and dynamical properties of the human insulin. The MD simulation results showed that depending on time evolution of integral characteristics such as the backbone root mean-square deviation, gyration radius, solvent accessible surface area, the root mean-square fluctuations and the secondary structure content, the examined

mutants can be tentatively divided into three groups: 1) the mutants His^{A8}, Val^{A10}, Ala^{B17}, Asp^{B25}, Thr^{B26}, Glu^{B27}, Glu^{A13+Glu^{B10}}, Glu^{B1+Glu^{B27}} and Glu^{B16+Glu^{B27}}, exerting a stabilizing effect on the protein structure in comparison with wild type insulin; 2) the mutants Gln^{B17}, Asp^{B10}, Ser^{B2+Asp^{B10}} and Glu^{A15+Asp^{A18}+Asp^{B3}} that did not significantly affect the dynamical properties of human insulin having a minimal stabilizing impact; 3) the mutants Asp^{B28}, Asp^{B9+Glu^{B27}}, Ser^{A13+Glu^{B27}} and Gln^{B18} destabilizing protein structure. The analysis of the time dependencies of the secondary structure content highlights the influence of Asp^{B28}, Asp^{B9+Glu^{B27}}, Ser^{A13+Glu^{B27}} and Gln^{B18} on the insulin unfolding. Moreover, our MD results indicate that substitution of the nonpolar residues in the insulin structure by hydrophilic ones caused the increase in protein stability in comparison with wild type protein.

ACKNOWLEDGEMENTS

This work was supported by the Ministry of Education and Science of Ukraine (the Young Scientist projects № 0120U101064 “Novel nanomaterials based on the lyophilic self-assembled systems: theoretical prediction, experimental investigation and biomedical applications” and the project № 0119U002525 “Development of novel ultrasonic and fluorescence techniques for medical micro- and macrodiagnostics”).

ORCID IDs

-  Olga Zhytniakivska, <https://orcid.org/0000-0002-2068-5823>;  Uliana Tarabara, <https://orcid.org/0000-0002-7677-0779>
 Valeriya Trusova, <https://orcid.org/0000-0002-7087-071X>;  Kateryna Vus, <https://orcid.org/0000-0003-4738-4016>
 Galyna Gorbenko, <https://orcid.org/0000-0002-0954-5053>

REFERENCES

- [1] Q. Hua, *Protein Cell*. **1**, 537-551 (2010), <https://doi.org/10.1007/s13238-010-0069-z>.
- [2] F. Hu, *Diabetes Care*. **34**, 1249-1257 (2011), <https://doi.org/10.2337/dc11-0442>.
- [3] M. Atkinson, G. Eisenbarth, and A. Michels, *The Lancet*. **383**, 69-82 (2014), [https://doi.org/10.1016/S0140-6736\(13\)60591-7](https://doi.org/10.1016/S0140-6736(13)60591-7).
- [4] M. Nakamura, Y. Misumi, T. Nomura, W. Oka, A. Isoguchi, K. Kanenawa, T. Masuda, T. Yamashita, Y. Inoue, Y. Ando, and M. Ueda, *Diabetes*. **68**, 609-616 (2019), <https://doi.org/10.2337/db18-0846>.
- [5] T. Nagase, K. Iwaya, K. Kogure, T. Zako, Y. Misumi, M. Kikuchi, K. Matsumoto, M. Noritake, Y. Kawachi, M. Kobayashi, Y. Ando, and Y. Katsura, *J. Diabetes Investig.* **11**, 1002-1005 (2020), <https://doi.org/10.1111/jdi.13199>.
- [6] Z.B. Taraghdari, R. Imani, and F. Mohabatpour, *Macromol. Biosci.* **19**, 1800458 (2019), <https://doi.org/10.1002/mabi.201800458>.
- [7] M. Akbarian, Y. Ghasemi, V. Uversky, and R. Yousefi. *Int. J. Pharm.* **547**, 450-468 (2018), <https://doi.org/10.1016/j.ijpharm.2018.06.023>.
- [8] L. Nielsen, R. Khurana, A. Coats, S. Frokjaer, J. Brange, S. Vyas, V.N. Uversky, and A.L. Fink, *Biochemistry*. **40**, 6036-6046 (2001), <https://doi.org/10.1021/bi002555c>.
- [9] M. Groenning, S. Frokjaer, and B. Vestergaard, *Curr. Protein. Pept. Sci.* **10**, 509-528 (2009), <https://doi.org/10.2174/138920309789352038>.
- [10] F. Librizzi, and C. Rischel, *Protein Sci.* **14**, 3129-3134 (2005), <https://doi.org/10.1110/ps.051692305>.
- [11] A. Podesta, G. Tiana, P. Milani, and M. Manno. *Biophys J.* **90**, 589-597 (2006), <https://doi.org/10.1529/biophysj.105.068833>.
- [12] S. Grudzielanek, R. Jansen, and R. Winter, *J. Mol. Biol.* **351**, 879-894 (2005), <https://doi.org/10.1016/j.jmb.2005.06.046>.
- [13] A. Noormägi, K. Valmsen, V. Tõugu, and P. Palumaa, *Protein J.* **34**, 398-403 (2015), <https://doi.org/10.1007/s10930-015-9634-x>.
- [14] J. Brange, L. Andersen, E. Laursen, G. Meyn, and E. Rasmussen, *J. Pharm. Sci.* **86**, 517-525 (1997), <https://doi.org/10.1021/js960297s>.
- [15] M. Ziaunys, T. Sneideris, and V. Smirnovas, *Phys. Chem. Chem. Phys.* **20**, 27638-276455 (2018), <https://doi.org/10.1039/C8CP04838J>.
- [16] M. Muzaffar, and A. Ahmad, *Plos ONE*. **20**, e27906 (2011), <https://doi.org/10.1371/journal.pone.0027906>.
- [17] I. Bekard, and D. Dunstan, *Biophys J.* **97**, 2521-2531 (2009), <https://doi.org/10.1016/j.bpj.2009.07.064>.
- [18] M. Sorci, R. Grassucci, I. Hahn, J. Frank, and G. Belfort, *Proteins*. **77**, 62-73 (2009), <https://doi.org/10.1002/prot.22417>.
- [19] C.G. Frankær, P. Sønderby, M.B. Bang, R.V. Mateiu, M. Groenning, J. Bukrinski, and P. Harris, *J. Struct. Biol.* **199**, 27-38 (2017), <https://doi.org/10.1016/j.jsb.2017.05.006>.
- [20] A. Noormagi, J. Gavrilova, J. Smirnova, V. Tõugu, and P. Palumaa, *Biochem. J.* **430**, 511-518 (2010), <https://doi.org/10.1042/BJ20100627>.
- [21] J. Hansen, *Biophys. Chem.* **39**, 107-110 (1991), [https://doi.org/10.1016/0301-4622\(91\)85011-E](https://doi.org/10.1016/0301-4622(91)85011-E).
- [22] A. Ahmad, V. Uversky, D. Hong, and A. Fink, *J. Biol. Chem.* **280** 42669-42675 (2005), <https://doi.org/10.1074/jbc.M504298200>.
- [23] M. Akbarian, R. Yousefi, A.A. Moosavi-Movahedi, A. Ahmad, and V.N. Uversky, *Biophys. J.* **117**, 1626-1641 (2019), <https://doi.org/10.1016/j.bpj.2019.09.022>.
- [24] D.P. Hong, A. Ahmad, and A.L. Fink, *Biochemistry*. **45**, 9342-9353 (2006), <https://doi.org/10.1021/bi0604936>.
- [25] D.P. Hong, and A.L. Fink, *Biochemistry*, **44**, 16701-16709 (2005), <https://doi.org/10.1021/bi051658y>.
- [26] R. Huang, N. Maiti, N. Philips, P.R. Carey, and M.A. Weiss, *Biochemistry*. **45**, 10278-10293 (2006), <https://doi.org/10.1021/bi060879g>.
- [27] M.I. Ivanova, S.A. Sievers, M.R. Sawaya, J.S. Wall, and D. Eisenberg, *PNAS*, **106**, 18990-18995 (2009), <https://doi.org/10.1073/pnas.0910080106>.
- [28] X.Q. Hua, and M.A. Weiss, *J. Biol. Chem.* **279**, 21449-21460 (2004), <https://doi.org/10.1074/jbc.M314141200>.
- [29] M. Bouchard, J. Zurdo, E.J. Nettleton, C.M. Dobson, and C.V. Robinson, *Protein. Sci.* **9**, 1960-1967 (2008), <https://doi.org/10.1110/ps.9.10.1960>.
- [30] V. Babenko, and W. Dzwolak, *FEBS Lett.* **587**, 625-630 (2013), <https://doi.org/10.1016/j.febslet.2013.02.010>.
- [31] L. Nielsen, S. Frokjaer, J. Brange, V.N. Uversky, and A.L. Fink, *Biochemistry*, **40**, 8397-8409 (2001), <https://doi.org/10.1021/bi0105983>.
- [32] S.A. Lieblich, K.Y. Fang, J.K.B. Cahn, J. Rawson, J. LeBon, H.T. Ku, and D.A. Tirrell, *J. Am. Chem. Soc.* **139**, 8384-8387 (2017), <https://doi.org/10.1021/jacs.7b00794>.
- [33] J. Huang, and A. MacKerell, *J. Comput. Chem.* **34**, 2135-2145 (2013), <https://doi.org/10.1002/jcc.23354>.
- [34] S. Jo, J. Lim, J. Klauda, and W. Im, *Biophys. J.* **97**, 50-58 (2009), <https://doi.org/10.1016/j.bpj.2009.04.013>.
- [35] T. Darden, D. York, and L. Pedersen, *J. Chem. Phys.* **98**, 10089-10092 (1993), <https://doi.org/10.1063/1.464397>.
- [36] W. Humphrey, A. Dalke, and K. Schulten, *J. Mol. Graph.* **14**, 33-38 (1996), [https://doi.org/10.1016/0263-7855\(96\)00018-5](https://doi.org/10.1016/0263-7855(96)00018-5).
- [37] T.S. Choi, J.W. Lee, K.S. Jin, and H.I. Kim, *Biophys. J.* **107**, 1939-1949 (2014), <https://doi.org/10.1016/j.bpj.2009.04.013>.

МОЛЕКУЛЯРНО-ДИНАМІЧНЕ ДОСЛІДЖЕННЯ МУТАНТІВ ІНСУЛІНУ

О. Житняківська, У. Тарабара, В. Трусова, К. Вус, Г. Горбенко

*Кафедра медичної фізики та біомедичних нанотехнологій, Харківський національний університет імені В.Н. Каразіна
м. Свободи 4, Харків, 61022, Україна*

Інсулін людини, невеликий гормон пептидної природи, що складається з А-ланцюга (21 залишок) та Б-ланцюга, які зв'язані між собою трьома дисульфідними містками, має важливе значення для контролю гіперглікемії при діабеті I типу. У даній роботі методом молекулярно-динамічного моделювання досліджено вплив 10 точкових мутацій (His^{A8}, Val^{A10}, Asp^{B10}, Gln^{B17}, Ala^{B17}, Gln^{B18}, Asp^{B25}, Thr^{B26}, Glu^{B27}, Asp^{B28}), 6 подвійних мутацій (Glu^{A13}+Glu^{B10}, Ser^{A13}+Glu^{B27}, Glu^{B1}+Glu^{B27}, Ser^{B2}+Asp^{B10}, Asp^{B9}+Glu^{B27}, Glu^{B16}+Glu^{B27}) та однієї потрійної мутації (Glu^{A15}+Asp^{A18}+Asp^{B3}) на структуру та динаміку інсуліну людини. З використанням програмного пакету GROMACS (версія 5.1) і силового поля CHARMM36m, було проведено серію 100 нс молекулярно-динамічних (МД) симуляцій дикого типу інсуліну людини (WT) та його мутантів при температурі 500 К. Результати МД моделювання були проаналізовані в термінах параметрів, що характеризують як глобальну так і локальну структуру білка, таких як середньоквадратичне відхилення остову ланцюга, радіус інерції, площа поверхні, доступна для розчинника, середньоквадратичні флуктуації та вміст вторинної структури. Результати молекулярно-динамічного моделювання продемонстрували, що в залежності від еволюції інтегральних характеристик, усі досліджені мутанти можна умовно розділити на три групи: 1) мутанти His^{A8}, Val^{A10}, Ala^{B17}, Asp^{B25}, Thr^{B26}, Glu^{B27}, Glu^{A13}+Glu^{B10}, Glu^{B1}+Glu^{B27} та Glu^{B16}+Glu^{B27}, що мають стабілізуючий вплив на структуру білка у порівнянні з диким типом інсуліну; 2) мутанти Gln^{B17}, Asp^{B28}, Asp^{B10}, Ser^{B2} + Asp^{B10} та Glu^{A15} + Asp^{A18} + Asp^{B3}, які істотно не впливали на динаміку білка або мали незначний стабілізуючий вплив; 3) мутанти Asp^{B9} + Glu^{B27}, Ser^{A13} + Glu^{B27} та Gln^{B18}, що дестабілізували структуру білка. При аналізі еволюції вторинної структури отримані докази впливу мутацій Asp^{B28}, Asp^{B9}+Glu^{B27}, Ser^{A13}+Glu^{B27} та Gln^{B18} на ступінь розгортання інсуліну. Результати МД демонструють, що заміна неполярних залишків в структурі інсуліну на гідрофільні, підвищує стабільність білка порівняно з інсуліном дикого типу.

КЛЮЧОВІ СЛОВА: людський інсулін, мутанти, молекулярно-динамічне моделювання, амілоїд.